Quantum Simulation of a 2D Quasicrystal with Cold Atoms

Nicolas Macé [1], Anuradha Jagannathan [1,*] and Michel Duneau [2]

[1]   Laboratoire de physique des Solides, Université Paris-Sud, 91405 Orsay, France; nicolas.mace@u-psud.fr
[2]   Centre de Physique Théorique, École Polytechnique, 91128 Palaiseau, France; duneau.michel@free.fr
*   Correspondence: jagannathan@lps.u-psud.fr; Tel.: +33-1-691-569-43

Abstract: We describe a way to obtain a two-dimensional quasiperiodic tiling with eight-fold symmetry using cold atoms. One can obtain a series of such optical tilings, related by scale transformations, for a series of specific values of the chemical potential of the atoms. A theoretical model for the optical system is described and compared with that of the well-known cut-and-project method for the Ammann–Beenker tiling. The relation between the two tilings is discussed. This type of cold atom structure should allow the simulation of several important lattice models for interacting quantum particles and spins in quasicrystals.

Keywords: quasicrystals; electronic properties

1. Introduction

With the discovery of the first quasicrystals [1], the quest began for, on the one hand, new quasiperiodic systems with better characterization of structural properties, and on the other hand, for theoretical methods to handle these systems. One of the goals of experiment has been, in particular, obtaining a single component quasicrystal, in the hope of finding direct relationships between its physical and geometrical properties. This may, we hope, become possible in cold atom systems. Cold atoms in optical lattices have been used to simulate quantum behavior of periodic crystals but not, thus far, of quasiperiodic tilings. Cold gases, of cesium, rubidium or potassium atoms for example, are used as quantum simulators for a great variety of systems. As compared to real solid state systems, cold atom systems represent ideal systems, in which model parameters can be tuned at will. Improvements in experimental techniques have resulted in an explosion of experimental simulations of condensed matter physics, quantum information and quantum optics models. Ultracold quantum gases in optical potentials therefore provide an exciting possibility towards the goal of synthesizing a perfect one-component quasicrystal.

The behavior of electrons in quasicrystals remains insufficiently understood, especially in dimensions higher than one. Numerical investigations have thus far been limited by the amount of computational time needed. Much effort has been devoted to trying to understand tight-binding models on simple tilings, as a first step towards the description of more realistic systems. It is thus natural to ask what possibilities exist for realizing a quasiperiodic tiling by trapping cold atoms in an optical potential. The advantages of such a system, if realized, are manifold. First, it would become possible to fabricate samples using a single atomic species—a significant simplification compared to real quasicrystals. It would be possible to directly observe the quantum states of the atoms, described by a tight-binding Hamiltonian. Finally, and importantly, many of the parameters of the hopping and interaction Hamiltonians could be tuned. Many body properties in quasiperiodic systems could be properly studied under controlled conditions. The amount of disorder could be tuned as desired, to mimic experimental situations. An experimental set-up to realize a two-dimensional tiling was

proposed in [2,3]. It was shown that one can obtain an eight-fold tiling bearing a close relation to the Ammann–Beenker tiling [4]. We will present the experimental system, the theoretical model and explain how a perfect quasiperiodic tiling can be obtained by introducing additional small interactions between atoms.

This paper begins with a description of the experimental set-up. We then introduce a 4D description of the optical tiling that is naturally suggested by the experimental geometry. We next show the relation between the optical tilings and the perfect Ammann Beenker tiling, and describe how to transform the former into the other. In conclusion, some directions for simulating important theoretical models are suggested.

2. Experimental Set-Up

Optical trapping of atoms by laser generated potentials has led to the artificial realization in experiments of many different kinds of models on lattices, in which particles can move and interact via experimentally controlled interactions [5]. Atoms can be trapped by laser light thanks to the dipole force acting on an atom due to the Stark effect in an off-resonance electric field. Under suitable assumptions concerning the decay rate Γ of the excited state (for more details, see the review), it can be shown that the potential energy landscape seen by the atom that has the form

$$V(\vec{r}) = v_0 I(\vec{r}) \tag{1}$$

where v_0 is a constant and $I(\vec{r})$ is the average value of the intensity at the position $\vec{r}$. Denoting the electric field by $\vec{E}$, $I(\vec{r}) = |\vec{E}(\vec{r})|^2$. The sign of the prefactor, v_0, depends on the polarizability of the atom, and this can be positive or negative depending on the frequency of the laser, ω_L, relative to the resonance frequency ω_0 for the atom [6]. The constant v_0 depends, among other parameters, on the laser detuning and is positive for blue-detuning ($\omega_L > \omega_0$) and negative for red-detuning ($\omega_L < \omega_0$). In other words, atoms experience a net force directed towards nodes (antinodes) of the laser intensity pattern if the detuning parameter $\Delta = (\omega_L - \omega_0)$ is positive (resp. negative). In this paper, we study this latter case, corresponding to atoms being attracted to maxima of the laser intensity pattern I. We note that, for large detuning, corrections will appear to this interaction potential due to non-conservative processes, and we will neglect these. Using this type of optical potential, it has been possible to simulate models defined on a large variety of periodic structures including the square, triangular, Kagome and other lattices. We will now consider a quasiperiodic structure with eight-fold symmetry obtained by this method.

We consider a region where standing waves have been set up using four laser beams oriented at 45° angles in the *x*–*y* plane, as shown in Figure 1. The wavelengths, λ, are the same for all the beams, as are their amplitudes. We will consider the situation where all the polarizations are perpendicular to this plane, allowing the amplitudes to sum up to an absolute maximum. The alternative choice, of using in-plane polarizations, yields smaller maxima of amplitudes, smaller contrast, and would therefore be less efficient in trapping particles. For the case of four standing waves, the intensity is given by:

$$I(\vec{r}) = I_0 \left[\sum_{n=1}^{4} \cos(\vec{k}_n.\vec{r} + \phi_n) \right]^2 \tag{2}$$

where $\vec{r} = (x, y)$ is the position vector of the points lying in the plane of the lasers. The four wave vectors are given by:

$$\vec{k}_n = k(\cos\theta_n, \sin\theta_n) \qquad \theta_n = \frac{(n-1)\pi}{4} \tag{3}$$

with $n = 1, ..., 4$, where $k = 2\pi/\lambda$. Notice that the four beams can have arbitrary different phase-shifts ϕ_n. As long as the relative phase shifts are maintained at some fixed arbitrary values, these phase shifts do not change the nature of the structures obtained, as discussed later.
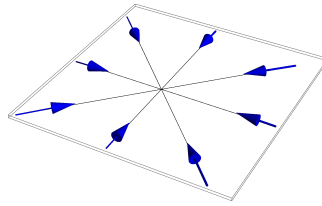
Figure 1. Schematic of experimental set-up with four standing waves at $\pi/4$ angles. The light is polarized perpendicularly to the plane of propagation.

The function $I(\vec{r})$ of Equation (2) is quasiperiodic since there is no integer relationship between the four wave vectors $\vec{k}_n$. The intensity landscape obtained for a random choice of the phases ϕ_n has a complex structure of maxima, minima and saddlepoints. The intensities of the peaks, or local maxima, have a range of values with the upper bound $I_{max} = 16I_0$. The potential energy thus has a minimum value of $V_{min} = -16V_0$ with $V_0 = |v_0|I_0$.

The cold atoms in this region are attracted to local maxima of $I(r)$—i.e., the local minima of the potential energy. If one now introduces a finite density of atoms, depending on the chemical potential, only maxima corresponding to intensities bigger than a cut-off I_c will be occupied by an atom. We will neglect fluctuations due to finite temperature and trapping of atoms in metastable configurations, and instead focus on the ideal structures one expects to find, as a function of I_c.

Figure 2 shows the optical tilings obtained for three representative values of the intensity cut-off: $I_c/I_0 = 10.8, 15$ and 15.82. The edge-length of the tiles can be seen to increase by a discrete scale factor, the irrational number $\alpha = 1 + \sqrt{2}$, also called the silver mean. The tilings are shown superposed on the intensity profile, represented by a shaded plot (dark shades for small intensity). These are examples of the type of structure that we will refer to as the optical quasicrystal (OT). As can be seen from the shape of the tiles, it is closely related to the standard Ammann–Beenker or octagonal tiling (ABT) [4,7] composed of squares and $45°$ rhombuses. For larger and larger values of the cutoff, approaching $16I_0$, only the largest maxima will be occupied, and the atomic density in the xy plane correspondingly decreases. As the cutoff takes on successive special values in the series given in the next section, the lattice vectors increase by powers of the irrational number α.
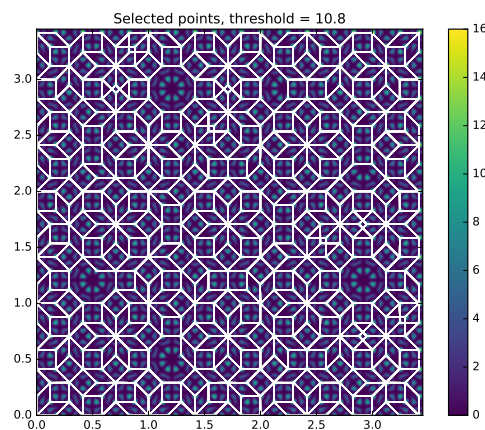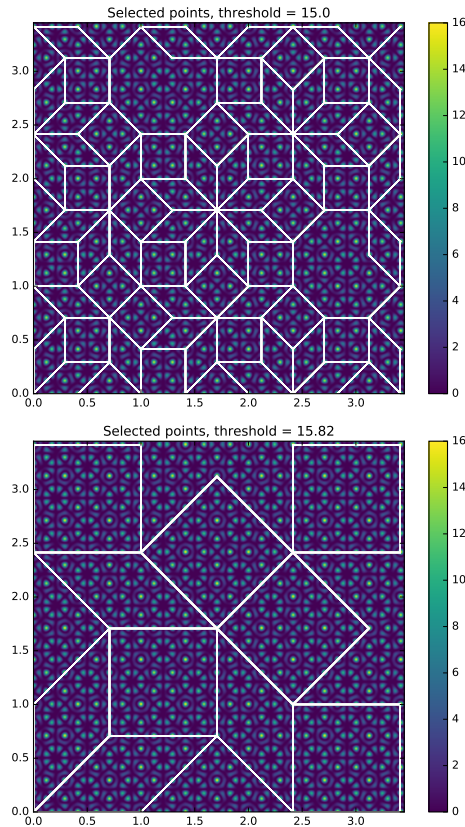

Figure 2. *Cont.*

Figure 2. Intensity plot showing the profile of the optical potential $I(\vec{r})$ in the plane. On this are superposed the tilings obtained by connecting occupied sites, for intensity cut-offs $I_c/I_0 = 10.8, 15.0$ and 15.82.

3. A Four-Dimensional Model for the Optical Quasicrystal

This section summarizes the model of the OT which was introduced in [2,3], along with some additional details, and clarifications. Our aim here will be to give a mathematical description of the optical tilings shown in Figure 2, and calculate quantities such as the lattice vectors in terms of the cutoff intensity I_c. In this model, the only dimensionful parameters are $\lambda = 2\pi/k$ the wavelength of the laser light, which sets the length-scale, and V_0, which sets the energy scale in the problem. All other relevant lengths and energies can then be specified in terms of these two quantities.

Let us return to the intensity of the laser beams given by the function Equation (2). Since the four vectors $\vec{k}_n$ have no rational relationships, $I(\vec{r})$ is a quasiperiodic function in the sense of Bohr [8] and Besicovitch [9]. The Fourier transform is readily obtained by expanding cosines so that the spectrum is the finite set of all combinations $\pm\vec{k}_n \pm \vec{k}_m$.

The eight-fold symmetry of $I(\vec{r})$ follows from the remark that a rotation γ (see [3]) of $\pi/4$ maps $\{\vec{k}_1, \vec{k}_2, \vec{k}_3, \vec{k}_4\}$ to $\{\vec{k}_2, \vec{k}_3, \vec{k}_4, -\vec{k}_1\}$ (see Figure 3). $I(\vec{r})$ is also invariant by the two-fold symmetry σ w.r.t. the x-axis, which maps $\{\vec{k}_1, \vec{k}_2, \vec{k}_3, \vec{k}_4\}$ to $\{\vec{k}_1, -\vec{k}_4, -\vec{k}_3, -\vec{k}_2\}$. While this C_{8v} symmetry is not crystallographic in 2D, it is crystallographic in the 4D space $\mathbb{R}^4$: Lifting γ and σ to $\mathbb{R}^4$ gives the integer matrices:

$$\Gamma = \begin{bmatrix} 0 & 0 & 0 & -1 \\ 1 & 0 & 0 & 0 \\ 0 & 1 & 0 & 0 \\ 0 & 0 & 1 & 0 \end{bmatrix}, \quad \Sigma = \begin{bmatrix} 1 & 0 & 0 & 0 \\ 0 & 0 & 0 & -1 \\ 0 & 0 & -1 & 0 \\ 0 & -1 & 0 & 0 \end{bmatrix} \tag{4}$$

in the standard basis $\{\vec{\varepsilon}_1, \vec{\varepsilon}_2, \vec{\varepsilon}_3, \vec{\varepsilon}_4\}$. They satisfy $\Gamma^8 = \Sigma^2 = I$ and $\Sigma\Gamma\Sigma^{-1} = \Gamma^{-1}$. This 4D representation of C_{8v} is reducible since $\mathbb{R}^4$ is the Cartesian product of two planes P and P' that are orthogonal and invariant. While the restriction of Γ to P is the previous γ rotation, the restriction to P' is a rotation γ' of $3\pi/4$.

One can choose orthonormal bases $\{\vec{e}_x, \vec{e}_y\}$ in P (the "physical space") and $\{\vec{e}'_x, \vec{e}'_y\}$ in P' (the "perpendicular space") so that the orthogonal projections $\vec{e}_n = \pi(\vec{\varepsilon}_n)$ and $\vec{e}''_n = \pi'(\vec{\varepsilon}_n)$, all of norm $1/\sqrt{2}$, are as shown in Figure 3.

Points $\vec{R} = (R_1, R_2, R_3, R_4)$ of $\mathbb{R}^4$ also write $(\vec{r}, \vec{r}') = (x, y, x', y')$ in the $\{\vec{e}_x, \vec{e}_y, \vec{e}'_x, \vec{e}'_y\}$ bases of $\mathbb{R}^4$. The transformation is given by the following rotation $\mathcal{R}$:

$$
\begin{bmatrix} x \\ y \\ x' \\ y' \end{bmatrix} = \mathcal{R} \begin{bmatrix} R_1 \\ R_2 \\ R_3 \\ R_4 \end{bmatrix} = \frac{1}{2} \begin{bmatrix} \sqrt{2} & 1 & 0 & -1 \\ 0 & 1 & \sqrt{2} & 1 \\ \sqrt{2} & -1 & 0 & 1 \\ 0 & 1 & -\sqrt{2} & 1 \end{bmatrix} \cdot \begin{bmatrix} R_1 \\ R_2 \\ R_3 \\ R_4 \end{bmatrix}
\tag{5}
$$

If $\vec{R} = (\vec{r}, \vec{r}')$ and $\vec{K} = (\vec{k}, \vec{k}')$ are two 4D vectors, then $\vec{K}.\vec{R} = \sum K_n R_n = \vec{k}.\vec{r} + \vec{k}'.\vec{r}'$.

The wave vectors $\vec{k}_n$ are the projections in P of orthogonal 4D vectors $\vec{K}_n = K\vec{\varepsilon}_n = (\vec{k}_n, \vec{k}'_n)$, so that their magnitude is $K = \sqrt{2}\,k$. The intensity Equation (2) can be obtained from the 4D periodic function

$$
\mathcal{I}(\vec{R}) = I_0 \left[\sum_{n=1}^{4} \cos(\vec{K}_n.\vec{R}) \right]^2
\tag{6}
$$

so that $I(\vec{r}) = \mathcal{I}(\vec{r}, 0)$ is the restriction of $\mathcal{I}(\vec{R})$ to the plane P.

The maxima of $\mathcal{I}(\vec{R})$ occur on points where all cosines equal 1, i.e. on the cubic lattice $\frac{2\pi}{K}\mathbb{Z}^4$, and on points where all cosines equal -1, which correspond to the body centers. Let B denote the BCC lattice of $\mathbb{Z}^4$: coordinates are either all integers or all half integers. Accordingly, the maxima $16I_0$ of $\mathcal{I}(\vec{R})$ are located on the BCC lattice $\frac{2\pi}{K}B = \frac{\sqrt{2}\pi}{k}B$. The vertices of B can be written as $\vec{R} = T\vec{x} = \sum x_n \vec{\beta}_n$ with $\vec{x} = (x_1, x_2, x_3, x_4)$ (where the x_n are integers) and where T is the matrix

$$
T = \frac{1}{2} \begin{bmatrix} 1 & -1 & -1 & -1 \\ 1 & 1 & -1 & -1 \\ 1 & 1 & 1 & -1 \\ 1 & 1 & 1 & 1 \end{bmatrix}
\tag{7}
$$

A basis of B is given by the unit vectors $\vec{\beta}_n = T\vec{\varepsilon}_n$ ($n = 1, .., 4$). One can check that $\det(T) = \frac{1}{2}$ and that $T.C_{8v} = C_{8v}.T$, so that B is invariant with respect to C_{8v} and belongs to the same Bravais class as the hypercubic lattice $\mathbb{Z}^4$. Furthermore, T commutes with the eight-fold generator Γ. The four primitive lattice vectors $\vec{\beta}_n$ of B project onto the set $\vec{b}_n$ in P, and $\vec{b}'_n$ in P', as shown in Figure 3. The norms of these vectors are $b_n = \frac{1}{2}\sqrt{2 + \sqrt{2}}$ and $b'_n = \frac{1}{2}\sqrt{2 - \sqrt{2}}$.
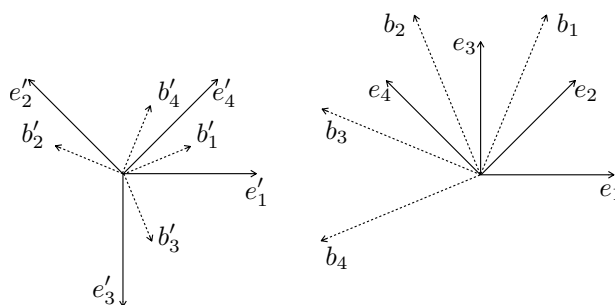

Figure 3. Projections of the bases $\{\varepsilon_n\}$ of $\mathbb{Z}^4$ and $\{\beta_n\}$ of the BCC lattice in P' (**left**) and P (**right**).

The condition $\mathcal{V}(\vec{R}) \leq V_c$ is equivalent to a condition $\mathcal{I}(\vec{R}) \geq I_c$. If the cutoff I_c is high enough, the last condition is fulfilled in a set of disjoint domains centered on the BCC lattice $\frac{\sqrt{2}\pi}{k}B$. If the cutoff I_c is close to the absolute maximum $I_m = 16I_0$, one can substitute the quadratic approximation $\mathcal{I}(\vec{R}) \approx (16 - 8k^2(\vec{r}^2 + \vec{r}'^2))I_0$. The domains are close to spheres of radius ρ given by $8k^2\rho^2 = (16I_0 - I_c)/I_0$. Their projections on P and P' are close to disks of the same radius.

If $I(\vec{r}) > I_c$ is a local maximum, the point $(\vec{r}, \vec{0})$ belongs to a domain centered on a vertex $\vec{R}$ of the BCC lattice, at a distance bounded by ρ in the quadratic approximation. These points $\vec{r}$ are close to the BCC lattice, allowing for a comparison with the cut-and-project method as discussed below.

The vertices of the octagonal tiling [7] are the projections $\vec{r}$ of 4D lattice points $\vec{R} = (\vec{r}, \vec{r}')$ such that $\vec{r}'$ belongs to an octagonal window generated by the four vectors $\vec{b}'_n$ (see [10] for the cut-and-project algorithm). The area of this window (see Figure 4) is $W = \frac{\sqrt{2}\pi^2}{k^2}$. The inflation transformation of the octagonal tiling enlarges the edge length of the tiles in P by a factor α, while distances in P' are reduced by the same factor. Inflated octagonal tilings correspond to selection windows of area W/α^{2p} with $p = 0, 1, 2, ...$
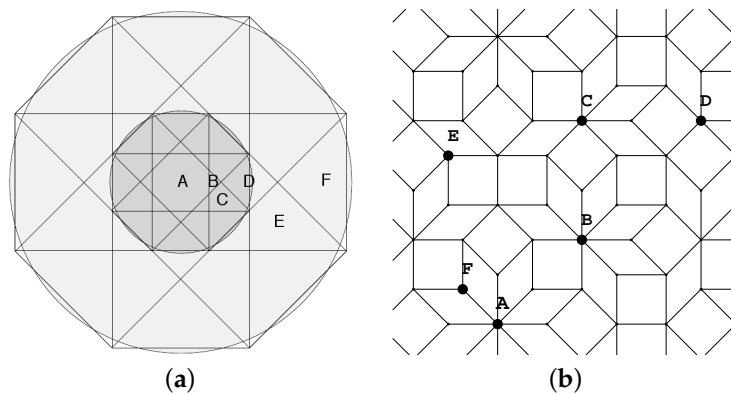

(**a**)　　　　　　　　　　　　　　　　　(**b**)

Figure 4. (**a**) the big octagon represents W, the selection window for the ABT in P'. Circles represent the selection windows D' for the OT for the values $p = 0$ and $p = 1$; (**b**) a portion of the OT with the corresponding local environments (A,B,...) corresponding to subwindows of the big octagon.

If V_c is low enough and if the areas of D' and W are equal (up to inflation), a relationship between both structures can be expected. This equality ensures that the two structures have the same density of points. Using the quadratic approximation of $\mathcal{I}(\vec{R})$, this condition writes:

$$\frac{V_c - 16\,V_0}{V_0} = \frac{16\,I_0 - I_c}{I_0} = 8\sqrt{2}\pi\alpha^{-2p} \tag{8}$$

The OT of Figure 2 corresponds to $p = 1, 2$ and 3. The circular windows D' are shown in Figure 4 for $p = 0$ and $p = 1$, inside the window of the octagonal tiling. The criterion in Equation (8) can be further simplified by noting that, for $p > 1$, the cosine terms in V can be expanded to second order in the distance ρ. In this limit, the selection windows for the OT are approximately circular and the radius for the cutoff value I_c is given by $k^2\rho_c^2 = \sqrt{2}\pi\alpha^{-2p}$. It can be shown that the edges of the tiles of the pth OT have length $\ell = \frac{\sqrt{2}\pi}{k}|b_n|\alpha^p$. The smallest edge length $\ell \approx 3.81\lambda$ is obtained for $p = 1$.

4. Fourier Transform of the OT

We now turn to the diffraction pattern of a structure obtained when atoms occupy all of the allowed vertices corresponding to a particular value of I_c. The general method for finding the Fourier transform and indexation of peaks is discussed for example by Katz and Gratias in [11]. The structure factor consists of Bragg peaks whose positions are given by the reciprocal lattice of the 4D cubic lattice, and whose peak intensities are given by the Fourier Transform of the selection window. Due

to the close similarity of their selection windows, the structure factor of the OT and that of the ABT are expected to be very similar, with peaks in the same positions but with slight differences in their intensities. Here, we will confine our attention to the indexing of Bragg peaks. It is interesting to observe that spherical selection windows were introduced by Grimm and Baake in the context of the diffraction patterns of quasiperiodic tilings [12], as a useful approximation in the calculation of the structure factor. For the optical quasicrystal, in contrast, we see that the spherical window turns out to be the correct, physically imposed choice, provided only that the cut-off I_c is large enough.

The 4D basis vectors are $\vec{K}_n = (2\sqrt{2}\pi/\lambda)\vec{\varepsilon}_n$. After projection in P, one obtains the four lattice vectors of Equation (3):

$$\vec{k}_n = \frac{2\sqrt{2}\pi}{\lambda}\vec{e}_n. \tag{9}$$

The peaks of the structure factor $S(\vec{k})$ are found at positions $\vec{k} = \sum h_n \vec{k}_n$ with the condition that

$$\exp(i\pi \sum_n h_n) = 1, \tag{10}$$

equivalent to the requirement that $\sum_n h_n$ be even. This condition is equivalent to saying that the positions of its Bragg peaks are those of $k\sqrt{2}F$, the reciprocal lattice of $\frac{\pi\sqrt{2}}{k}B$, after projection into P. The values of the intensities are determined by the Fourier transform of the selection window, which is of octagonal shape for the ABT, and circular shape for the OT. The resulting differences between the two structure factors would show up only under a detailed comparison of peak intensities. Figure 5 shows the eight vectors $\pm\vec{k}_n$, and the numerically calculated intensity function $S(\vec{k})$ defined by

$$S(\vec{k}) = \frac{1}{N}\sum_{i,j}\exp[i\vec{k}.(\vec{r}_i - \vec{r}_j)], \tag{11}$$

where N is the number of sites in the sample. The set of intense peaks nearest the origin correspond to the combinations $\{\pm1, \pm1, 0, 0\}$ and permutations thereof, in accordance with the condition in Equation (10). The structure factors of successive OT for $p \geq 1$ will be the same, only rescaled by powers of α^{-p}, to take into account the inflation in real space.
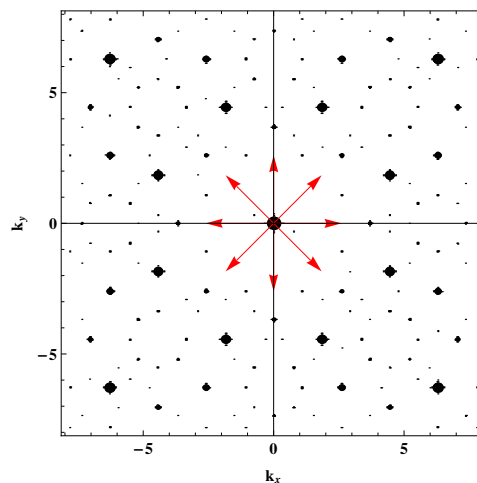

Figure 5. The structure factor calculated using Equation (11) for a sample of 4000 sites of the optical quasicrystal ($p = 0$). Intensities of the peaks are proportional to the area of the spots, and k_x and k_y are given in units of λ^{-1}. Arrows indicate the eight shortest reciprocal lattice vectors.

5. From the Optical Tiling to the Ammann–Beenker Tiling

In the preceding discussion, we assumed that when atoms are loaded into this optical potential, they occupy sites of lowest potential energy i.e., highest intensity, at very low temperature, giving

rise to the optical tiling. While overall, the intensities of the occupied peaks vary within the range $I_{max} > I > I_c$, one can define different categories of sites. It is easily seen that the typical value of the potential energy depends on the local environment, as follows. For convenience, we will describe the environment of each site by the letter A,B,... as determined by its position in the octagonal acceptance window W (see Figure 4), and for purposes of illustration, we consider the OT for $p = 1$. Figure 6 is a contour plot of the intensity $I(\vec{r})$ in perpendicular space. The value of the potential on a given site depends on its perpendicular coordinate, decreasing with the distance from the origin. For the values of the potential shown, these contours are close to circular. On the other hand, as we saw (in Figure 4), the distance from the origin in perpendicular space coordinate tends to get larger as z decreases. As shown in Figure 6, the high coordination number sites ($8 > z > 5$) sites correspond to the region inside the small red octagon, and these have the highest values of intensity, $16 > I/I_0 >\approx 15$. The sites with small coordination numbers, which lie in the region between the red and black octagons, have values in the range $15 >\approx I/I_0 >\approx 11$.
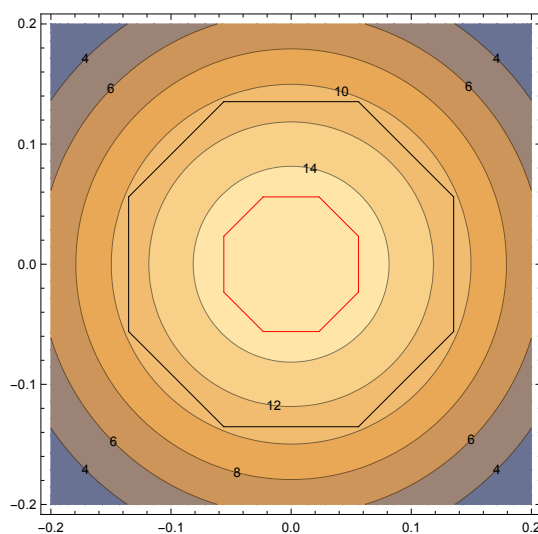

Figure 6. Contour plot of the intensity of peaks as a function of the perpendicular space coordinates. The **black** octagon delimits the region corresponding to all sites of the $p = 1$ OT, and the **red** octagon delimits the region corresponding to $z \geq 5$ sites.

We turn now to the problem of structure differences between the Ammann–Beenker tiling and the optical tiling. These arise from the difference in shape of their acceptance windows in perpendicular space. Comparing the two acceptance domains, one sees that they overlap over most of the regions that they occupy. This ensures that a large fraction of the selected points are identical in the two tilings. The differences between the two windows arise in the outlying regions. Firstly, the difference in the selection window has the result that some sites that are present in the AB tiling are missing in the OT. This leads to the empty hexagons and larger n-gons that one sees in Figure 2. Secondly, pairs of "twin-sites" separated by a very short distance δ appear in the OT, whereas in the AB tiling only one of the members of these pairs is present, the other being related by a "phason-flip". These two types of differences are shown in detail in Figure 7. Differences of intensity of the occupied and unoccupied sites are too small to be detected visually. For example, in Figure 7a, the intensities of the twin-sites are $10.8V_0$ (left site) and $11.1V_0$ (right site). Similarly, in Figure 7b, the intensities of the bright spots in the center of the vacant hexagonal region are $10.5V_0$ and $10.6V_0$. We note that the two defects shown in Figure 7 are situated on the same vertical worm of the ABT.
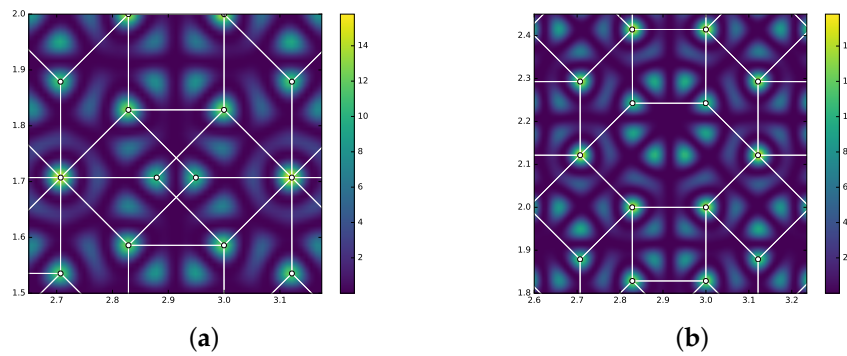
Figure 7. Two close-ups showing the intensity variation in the neighborhood (**a**) of a pair of twin-sites and (**b**) of an empty hexagon of the optical quasicrystal.

In summary, the difference in the shape of the selection windows leads to the appearance of inhomogeneities: as compared to the AB tiling, the OT has larger density fluctuations. The local intensity for the members of a pair of twin-sites are slightly different because their distances from the origin in perpendicular space are slightly different, as shown in Figure 8. Similarly, it is easy to show that the "vacant" site inside, say, an empty hexagon has a local intensity that lies just below the cut-off value.
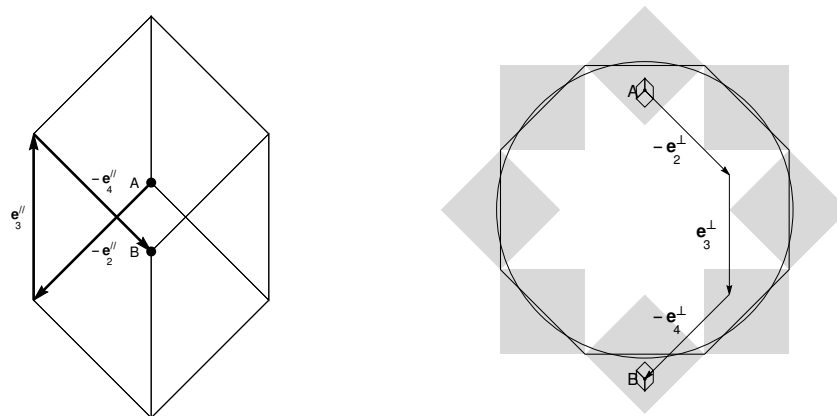

Figure 8. A pair of twin-sites in real (**left**) and in perpendicular space (**right**). In each case, the three lattice displacement vectors connecting the members of the pair are shown. Grey areas represent the total zones of existence of the two sites.

Small local fluctuations could lead to depopulating the twin-sites on the one hand, and populating the empty sites, on the other. This suggests that a way to remove the observed defects in the OT would be to turn on small short-range repulsive interactions between atoms. One can, indeed, tune the local interaction strengths between atoms in cold gases using Feshbach resonances [5]. In the standard Hubbard model for fermions, the interaction energy is nonzero when the two fermions are on a single site. In the extended Hubbard model, the interaction terms concern particles on nearest neighbor sites. Both kinds of terms can be simulated in cold atom gases. By varying the relative strength of the hopping and onsite interaction terms, it is possible, for example, to induce a superfluid to Mott insulator transition in a bosonic system [13]. Extensions of the Hubbard model to further near neighbors are reviewed in [14].

Adding a small short-range repulsive interaction energy will make it unfavorable to occupy simultaneously both sites of the twin pairs. One of the atoms corresponds to a larger distance from the origin in perpendicular space, and therefore has a slightly higher onsite energy than its twin.

It will therefore move to an unoccupied site with similar onsite energy, corresponding to one of the empty polygons. Let us make the reasonable assumption that all pairwise nearest neighbor interactions are negligible, except for those between the atoms on twin-sites. Let the strength of the repulsive energy for a pair of twin-sites be U'. Increasing U' will make it increasingly unfavorable to occupy simultaneously both sites of a twin pair. The U' value needed to shift an atom to an empty site can be estimated by the following argument. Consider a pair of twin-sites, whose positions in the perpendicular space are known, for example as in Figure 8. We now consider the change in the energy of the system ΔE if one of the twin-sites is vacated by the atom, which migrates to a defect "vacant" site. In this move, an atom is removed from the site whose coordinate $\vec{r}'_1$ lies within the cutoff radius but outside the octagonal window, and it is replaced elsewhere, on a site whose coordinate $\vec{r}'_2$ lies outside the cutoff radius but within the octagonal window. Such a move costs potential energy, and the change can be calculated by using the projected form of the potential energy in perpendicular space:

$$\Delta V = -16V_0 \sum_j \cos(\vec{k}'_j.\vec{r}'_2) - \cos(\vec{k}'_j.\vec{r}'_1) \approx 8V_0 k^2(\rho_2^2 - \rho_1^2) \tag{12}$$

where ρ_1 and ρ_2 are the radial distances of the initial and final positions of the atom in perpendicular space, and where we used the quadratic approximation of the potential. One can calculate the maximum value of this difference, by taking ρ_1 to be on the midpoint of an edge of the octagonal window, and ρ_2 on a vertex. The difference of distances can then be readily calculated, as a function of p. One thus finds that $\frac{\Delta V}{V_{max}} < \frac{\pi^2}{16}(2 - \sqrt{2})\alpha^{-2p}$. In order for such a hop to occur, the gain in onsite potential energy has to be compensated by the reduction of energy due to the destruction of a twin pair, namely, U'. This argument provides an upper bound to the value of the repulsive interaction needed to eliminate twin pairs. For $p = 1$, for example, one gets $U'/V_{max} \sim \Delta V/V_{max} \leq 0.06$, and the values for larger p are even smaller. This estimate shows that the repulsive interaction needed would be quite small relative to the onsite potential energy term.

To transform the OT into the AB tiling, in summary, one must introduce a small additional nearest neighbor interactions, over and above the optical potential. As we noted, in cold atom systems, such repulsive interactions can be introduced and experimentally controlled. The experimental set-up with the laser potential and repulsive interactions appears to be a feasible proposition for obtaining a perfect defect-free Ammann–Beenker tiling, at least in principle. In practice, there will be problems associated with slow dynamics, trapping in metastable configurations, and thus possibly a certain amount of disorder at finite temperatures.

The dynamics of this system can be described, to good approximation, by a tight-binding model, using the basis set of the Wannier states defined on the local minima of the optical lattice. As we have already pointed out, the values of the diagonal terms (the onsite energies), depend on the local environment (coordination number). The degree of localization of the Wannier functions depends on the depth of the potential minimum, and also varies to a limited extent. As for the hopping amplitude between two neighboring sites, they depend on several factors: on the distance between the sites, on the profile of the potential, and on the degree of localization of the local Wannier orbitals. These amplitudes will, therefore, have a variation of values for different pairs of sites. To evaluate the size of the spread of values, a detailed calculation is necessary. However, it can be argued, as in [3], that the hopping amplitudes are expected to fall off quickly with the distances and that the two important processes correspond to hopping along edges and across the small diagonal of the rhombus.

With the experimental and theoretical caveats mentioned above, we see that it is theoretically possible to simulate tight-binding Hamiltonians for fermions and bosons on a perfect octagonal tiling. This quasiperiodic tiling has been a subject of theoretical investigation since the mid-eighties. To cite only a few representative works, spectral properties and quantum dynamics in tight binding Hamiltonians have been investigated by many authors using a variety of techniques [15–19]. Many body effects in quasicrystals are also a question of current interest. The effect of Hubbard interactions [20], and, more recently, the fate of a local magnetic impurity [21] in this tiling, were

examined, motivated by recent experimental work in heavy fermion quasicrystal compounds [22,23]. It should be possible also to simulate and study the 2D quasiperiodic antiferromagnetic Heisenberg spin model, for which theoretical works have predicted novel ground state properties [24]. Effects of disorder, magnetic fields, etc. could also be systematically studied by means of a cold atom simulation.

6. Conclusions

We have outlined a method of obtaining a two-dimensional quasicrystal namely, the Ammann Beenker tiling, by trapping cold atoms in a laser generated potential. This would allow, for the first time, experimental studies of important theoretical paradigms for quasicrystals. The study of dynamics of fermions or bosons in a perfect 2D quasicrystal, and described by a Hubbard model, is one example. Another example is the experimental realization of the Heisenberg spin model. Disorder and effects due to magnetic perturbations could be investigated under controlled conditions. Progress in these problems would significantly advance our understanding of the thermodynamic and transport phenomena in real quasicrystals.

Author Contributions: All authors contributed equally to this manuscript.

Conflicts of Interest: The authors declare no conflict of interest.

References

1. Gratias, D.; Shechtman, D.; Blech, I.; Cahn, J.W. Metallic phase with long-range orientational order and no translational symmetry. *Phys. Rev. Lett.* **1984**, *53*, 1951.
2. Jagannathan, A.; Duneau, M. An eightfold optical quasicrystal with cold atoms. *Europhys. Lett.* **2014**, *104*, 6.
3. Jagannathan, A.; Duneau, M. The eight-fold way for optical quasicrystals. *Eur. Phys. J. B* **2014**, *87*, 1–10.
4. Beenker, F.P.M. *Algebraic Theory of Non Periodic Tilings of the Plane by Two Simple Building Blocks: A Square and a Rhombus*; TH Report 82-WSK-04; Eindhoven University of Technology: Eindhoven, The Netherlands, 1982.
5. Bloch, I.; Dalibard, J.; Zwerger, W. Many-body physics with ultracold gases. *Rev. Mod. Phys.* **2008**, *80*, 885.
6. Grimm, R.; Weidemüller, M.; Ovchinnikov, Y. Optical dipole traps for neutral atoms. *Adv. At. Mol. Phys.* **2000**, *42*, 95–170.
7. Janot, C.; Dubois, J.M. *Quasicrystalline Materials*; World Scientific: Singapore, 1988.
8. Bohr, H. *Almost Periodic Functions (AMS Chelsea Publishing)*; American Mathematical Society: Providence, RI, USA, 1947.
9. Besicovitch, A.S. *Almost Periodic Functions*; Dover Publications: Mineola, NY, USA, 1954.
10. Duneau, M.; Katz, A. Quasiperiodic patterns. *Phys. Rev. Lett.* **1985**, *54*, 2688.
11. Hippert, F.; Gratias, D. *Lectures on Quasicrystals*; Les Ulis: France, 1994.
12. Grimm, U.; Baake, M. *Aperiodic Order*; Cambridge University Press: Cambridge, UK, 2013; Volume 1.
13. Jaksch, D.; Bruder, C.; Cirac, J.I.; Gardiner, C.W.; Zoller, P. Cold bosonic atoms in optical lattices. *Phys. Rev. Lett.* **1998**, *81*, 3108.
14. Dutta, O.; Gajda, M.; Hauke, P.; Lewenstein, M.; Lühmann, D.S.; Malomed, B.A.; Sowiński, T.; Zakrzewski, J. Non-standard Hubbard models in optical lattices: A review. *Rep. Prog. Phys.* **2015**, *78*, 066001.
15. Sire, C.; Bellissard, J. Renormalization group for the octagonal quasi-periodic tiling. *Europhys. Lett.* **1990**, *11*, 439.
16. Benza, V.G.; Sire, C. Band spectrum of the octagonal quasicrystal: Finite measure, gaps, and chaos. *Phys. Rev. B* **1991**, *44*, 10343.
17. Passaro, B.; Sire, C.; Benza, V.G. Anomalous diffusion and conductivity in octagonal tiling models. *Phys. Rev. B* **1992**, *46*, 13751.
18. Zhong, J.X.; Mosseri, R. Electronic properties of the octagonal tiling: a new renormalization-group calculation. *J. Phys. I (Fr.)* **1994**, *4*, 1513–1525.
19. De Lassardiere, G.T.; Oguey, C.; Mayou, D. Breakdown of semi-classical conduction theory in approximants of the octagonal tiling. *Philos. Mag.* **2011**, *91*, 2778–2786.
20. Jagannathan, A.; Schulz, H.J. Magnetic states induced by electron-electron interactions in a plane quasiperiodic tiling. *Phys. Rev. B* **1997**, *55*, 8045.

21. Andrade, E.C.; Jagannathan, A.; Miranda, E.; Vojta, M.; Dobrosavljević, V. Non-Fermi-liquid behavior in metallic quasicrystals with local magnetic moments. *Phys. Rev. Lett.* **2015**, *115*, 036403.

22. Watanuki, T.; Kashimoto, S.; Kawana, D.; Yamazaki, T.; Machida, A.; Tanaka, Y.; Sato, T.J. Intermediate-valence icosahedral Au-Al-Yb quasicrystal. *Phys. Rev. B* **2012**, *86*, 094201.

23. Deguchi, K.; Matsukawa, S.; Sato, N.K.; Hattori, T.; Ishida, K.; Takakura, H.; Ishimasa, T. Quantum critical state in a magnetic quasicrystal. *Nat. Mater.* **2012**, *11*, 1013–1016.

24. Wessel, S.; Jagannathan, A.; Haas, S. Quantum antiferromagnetism in quasicrystals. *Phys. Rev. Lett.* **2003**, *90*, 177205.